

On the Power Saving in High-Speed Ethernet-based Networks for Supercomputers and Data Centers

Miguel Sánchez de la Rosa^a, Francisco J. Andújar^b, Jesus Escudero-Sahuquillo^a, José L. Sánchez^a, Francisco J. Alfaro-Cortés^a

^a*Department of Computing Systems, Universidad de Castilla-La Mancha, Avda. de España, Albacete, 02071, Castilla-La Mancha, Spain*

^b*Departamento de Informática, Universidad de Valladolid, Plaza de Santa Cruz, 8, Valladolid, 47002, Castilla y León, Spain*

Abstract

The increase in computation and storage has led to a significant growth in the scale of systems powering applications and services, raising concerns about sustainability and operational costs. In this paper, we explore power-saving techniques in high-performance computing (HPC) and datacenter networks, and their relation with performance degradation. From this premise, we propose leveraging Energy Efficient Ethernet (EEE), with the flexibility to extend to conventional Ethernet or upcoming Ethernet-derived interconnect versions of BXI and Omnipath.

We analyze the PerfBound proposal, identifying possible improvements and modeling it into a simulation framework. Through different experiments, we examine its impact on performance and determine the most appropriate interconnect. We also study traffic patterns generated by selected HPC and machine learning applications to evaluate the behavior of power-saving techniques.

From these experiments, we provide an analysis of how applications affect system and network energy consumption. Based on this, we disclose the weakness of dynamic power-down mechanisms and propose an approach that improves energy reduction with minimal or no performance penalty. To our knowledge, this is the first power management proposal tailored to future Ethernet-based HPC architectures, with promising results.

Keywords: Interconnection Networks, Energy efficiency, High Performance Computing, Power Efficiency, BXIv3

1. Introduction

Supercomputers and data centers are a critical infrastructure for IT applications and services. The demand for increasing computing power and storage capacity from fields like Physics, Chemistry, Biology, or Medicine requires not only raw computing power, but also sophisticated and efficient supercomputers and data centers that provide the highest performance out of the available resources. The emergence of generative AI has produced a steep increase in computational demand, and it is expected to further expand and permeate into other fields and services. However, the high-performance computing demand comes at the cost of power consumption. Energy and environmental constraints must be considered when planning the infrastructure that powers the backbones of the mentioned applications and services.

Energy consumption in supercomputers and data centers is the sum of power drawn, among other elements, by computing and storage nodes, the interconnection network, and the cooling system. Considering the most powerful supercomputers, the Exascale barrier was first overrun by the Frontier supercomputer, which remained the first in the TOP500 ranking [35] since June 2022, until El Capitan surpassed it in November 2024. Table 1 contains five of the most powerful supercomputers (in terms of computing power) with energy efficiency information supplied as per the last ranking. Energy efficiency is the ratio between the maximum performance and the average power consumption; the higher it is, the better. As we can see, the highest energy efficiency is achieved by the JUPITER booster machine, which is #4 in the ranking as of June 2025.

Rank	Name	Rmax [PFlop/s]	Power [MW]	Energy Efficiency [GFlops/Watts]
1	El Capitan	1742	29.58	58.89
2	Frontier	1353	24.61	54.98
3	Aurora	1012	38.7	26.15
4	JUPITER Booster	793.4	13.09	60.62
6	HPC6	477.9	8.46	56.48

Table 1: Power consumption and energy efficiency in the first five ranks of TOP500.

The operational costs for supercomputers are concerning because of power availability and sustainability reasons. Green500 [34] ranks TOP500 systems according to their power efficiency rather than the raw performance. If we examine the Green500 ranking for that date, we can see that the aforementioned systems are, in terms of power efficiency, in ranks #13, #42, #68,

and #12, respectively. Of course, designing a system with high regard for power efficiency leads to lower operational costs, namely in electricity.

Processors and accelerators used in the most powerful supercomputers have special mechanisms for reducing power consumption when thermal or power constraints are present. Intel processors, for example, introduced the C-states in the Sandy Bridge architecture [26] for advanced power management techniques. CPUs have several states defined, providing lower power consumption at the cost of performance and latency. Operating systems can indicate to the processor to enter a lower power state. However, changing states involves microarchitectural operations and voltage transitions, increasing latencies. During state transition times, CPUs execute no code, affecting performance. Still, even the most energy-saving states consume power. These features aim to keep CPU energy consumption proportional to the usage.

In this context, as computing nodes become more energy proportional, the interconnection network can become a significant fraction of computing system power [1]. Therefore, it is also necessary to design high-performance interconnection networks whose energy consumption is proportional to the traffic they carry and the rest of the system elements (e.g., processors, storage, etc).

Mainly, the opportunities for power savings come from periods of inactivity that would allow us to set ports to power-saving states. This would make power consumption more proportional to the network usage. If we look at the network usage for several applications, we can see that network activity fluctuates during execution. Periods of low network usage are good opportunities for applying power-saving techniques. Figure 1 shows the inactivity periods for a specific port on several applications when executed on our target simulated environment. The data is then used to form a histogram of 200 fixed-sized bins. Each bin i stores the number of registered inactivity periods that last between $width_{bin} \times i$ and $width_{bin} \times (i + 1)$ seconds. In these plots, we show values up to the 99th percentile for visibility reasons. On the x axis, we show the length of an inactivity period on that port. The left y_1 axis in black shows how many periods of inactivity are within the specified bin, and on the right, y_2 in red shows the cumulative distribution for every bin. In other words, the percentage of the histogram “area” below the bin. Regardless of the distribution on inactivity periods, any power-saving mechanism should take advantage of the longer periods to provide as much energy savings as possible. Moreover, we expect the performance penalty of the mechanism to be as low as possible or within a reasonable margin.

This paper explores the effects of network power management strategies on the performance of interconnection networks. First, we describe the background concepts in network energy reduction (see Section 2). Next, we describe the network power for large Ethernet-based interconnection networks used in supercomputers and data centers, and how it can be applied to BXIV3-based networks (see Section 3). We also show that more efficient interconnection networks are required to achieve energy proportionality. Afterwards, we describe the power model for BXIV3 that we have designed and the proposed energy-saving strategies. This model has been implemented in a powerful simulation framework, allowing large-scale network simulations. Furthermore, we have performed a set of simulation experiments (see Section 4) that show that, with the proposed power model strategies, the network power can be lowered without gravely affecting the overhead on execution time or latency. In particular, we managed to save more than 5 % of energy on the network by focusing on links only, while still outperforming other previous proposals in terms of performance overhead. We manage to improve the PerfBound [28] technique, even to the point of reverting power increases and resulting in actual savings. In our opinion, this is a promising start, given that our proposal and assumptions could be portable to future interconnection network technologies, such BXIV3 and the upcoming (Formerly Intel's) Omnipath¹ [8].

Mainly, the opportunities for power savings come from periods of inactivity that would allow us to set ports to power-saving states. This would make power consumption more proportional to the network usage. If we look at the network usage for several applications, we can see that network activity fluctuates during execution. Periods of low network usage are good opportunities for applying power-saving techniques. Figure 1 shows the inactivity periods for a specific port on several applications when executed on our target simulated environment. The data is then used to form a histogram of 200 fixed-sized bins. In these plots, we show values up to the 99th percentile for visibility reasons. On the x axis, we show the length of an inactivity period on that port. The left y_1 axis in black shows how many periods of inactivity are within the specified bin, and on the right, y_2 in red shows the cumulative distribution for every bin. In other words, the percentage of histogram "area" below the bin.

¹https://www.theregister.com/2025/06/09/omnipath_is_back/

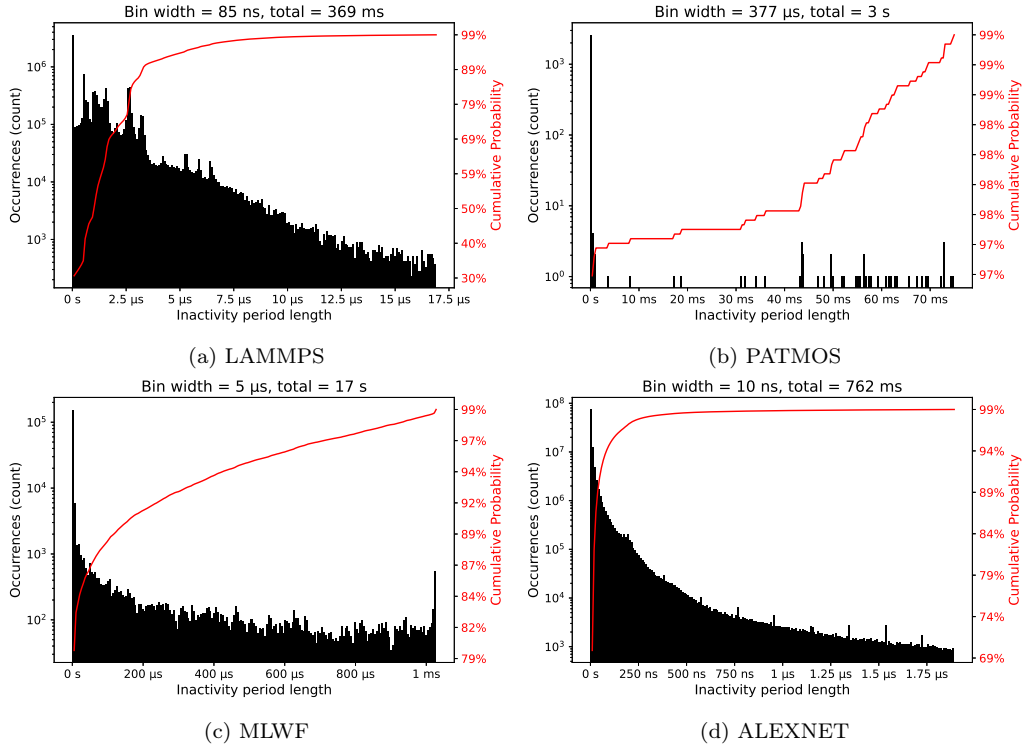


Figure 1: Inactivity histogram for a port when executing different applications.

In summary the main contributions of this paper are the following:

- Study of the power consumption and efficiency in HPC interconnection networks.
- Exploration of proposals to reduce link power draw in said networks, tailored to HPC and datacenter workloads.
- Study and implementation discussion of PerfBound [28] in our network simulator.
- A proposal (PerfBoundCorrect) to mitigate the oversights and implementation details of PerfBound.

2. Background

2.1. Energy consumption in high-speed interconnection networks

Network performance is affected by several network design issues, such as the topology, routing, flow control, and operating frequency, among others. Thus, designing an efficient and cost-effective network is crucial to guarantee the performance of the entire supercomputer and datacenter, as well as a balance between this performance and the investment and operational costs. Regarding HPC network technologies, a quick look into the TOP500 list shows us that Gigabit Ethernet, in various revisions, is present in many systems (32.8 %), only second to Infiniband (54.2 %). Such is the momentum of Ethernet in these environments that technologies like iWarp [10] and RoCE (RDMA over Converged Ethernet) [24] are working towards providing Ethernet with RDMA, present in interconnects like Infiniband.

Despite the notable capital investment for the equipment (CAPEX), operation costs (OPEX) and energy constraints are also relevant. The most notable examples of OPEX in HPC are power supply, cooling, and maintenance. Saving energy to reduce OPEX is being tackled by reducing power consumption (at the potential cost of performance), and cooling requirements are proportional to power consumption and thus, heat dissipation. The sheer scale of HPC environments implies huge CAPEX and OPEX. Electricity costs can be a deciding factor for HPC environments. Therefore, it is no surprise that power consumption reduction is sought, especially when examining the sparse network access in scientific applications. In fact, InfiniBand, the most pervasive interconnect in HPC, has power-saving mechanisms [13]. The ubiquity of Ethernet in other commercial areas has also caused several proposals to appear for Ethernet as well [17, 18]. The IEEE Task Force assembled to provide the technology with a common standard, resulting in the standard IEEE 802.3az, also known as Energy Efficient Ethernet (EEE).

Several design and operation strategies have been applied to reduce energy consumption in interconnection networks. Specifically, network energy consumption can be reduced by designing networks with high-radix switches. By increasing the switch radix, fewer routers are required. As switches aggregate more components, this also reduces the number of hops [20]. Consequently, the number of links in the network is reduced when the hop count is lower. Routing algorithms can also be relevant to energy consumption if additional links provide several paths between two nodes. Of course, these links will consume energy when unused.

On the other hand, operation cost (OPEX) in HPC environments increases as more network elements and nodes are added. Like with processors, network energy consumption could be reduced when the network is not being used. Periods of inactivity are determined by the communication pattern of applications. Scientific simulations attempt to minimize inter-node communication, with sparse bursts of network activity. On the other hand, in data centers, we can find deep learning applications, distributed storage, cloud computing, and data-intensive applications (e.g., search engines). The network load for this second set of applications depends on user requests, which need to be served as soon as possible to reduce perceived latency by end users [5].

Ethernet network links are traditionally always on, available to be used up to maximum speed. While on, ports frequently communicate to maintain alignment and synchronization. However, if links are switched to a power-saving state, energy could be saved over long network inactivity periods. Various techniques or strategies have been proposed to address this issue, some of which are described in the following sections.

2.2. Initial attempts for reducing link power consumption

The power consumption of any device can be divided into static and dynamic power. The later depends on clock frequency, supply voltage and transistor technology. Power consumption is roughly proportional to the cube of the frequency, which is promising for power saving. Dynamic Voltage and Frequency Scaling (DVFS) adjust voltage and frequency based on network utilization to save energy during idle periods and maintain performance under load. Implementations like Adaptive Supply Serial Links (ASSL) adjust supply voltage dynamically, though hardware complexity and additional circuitry such as voltage regulators are required [19, 30]. This conflicts with the objectives of interconnection networks being simple.

Since network technologies have gone through several revisions and can usually work at previous-generation data rates, this was thought to be a good strategy for energy saving. Adaptive Link Rate (ALR) aims to accomplish this by lowering link rates during periods of low utilization without altering voltages or frequencies directly. Instead, links can negotiate lower speeds. Although it can significantly save power, switching link rates introduces latency due to MAC handshakes, PHY configuration, and resynchronization [17], making implementation complex and limiting practical adoption. This is

detrimental in HPC environments because it can turn the network into a bottleneck when it is more needed.

2.3. Low Power Idle (LPI)

As ALR proved inefficient, Low Power Idle (LPI) [18] was proposed. LPI turns components off during inactivity periods instead of modifying the link frequency, which was more suitable. The corresponding states for links are *Wake* for ports active for transmission, and *Sleep* for inactive ports in a power-saving state. The underlying idea is that higher data rates provide the most energy-efficient transmission in terms of Joules per bit. Contrary to ALR, the switch between *Wake* and *Sleep* states occurs in microseconds instead of nanoseconds. Figure 2 shows these states and how they relate to packet transmissions. Note that t_w corresponds to the time to switch the port from *Sleep* to *Wake*, and t_s for the opposite transition. Specific values for these transition times on different Ethernet revisions are displayed in Table 2 [32].

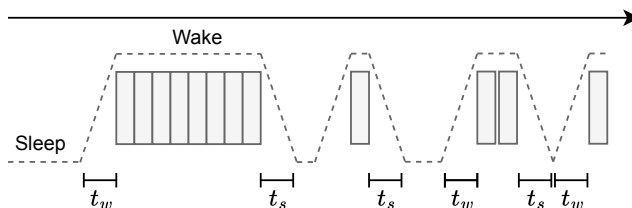


Figure 2: Port switching between *Wake* and *Sleep* states due to packet transmissions.

This figure shows that the link state starts at *Sleep*, and at a certain time, it starts transitioning to its *Wake* state. After t_w , the link is active and able to send several packets. Once the link has finished the transmission, it returns to *Sleep*. Note that every packet burst happening while the link is in *Sleep* state spends t_w waiting for the link to transition, regardless of the burst size. Then, longer messages are more efficient to transmit because fewer state transitions occur. On the contrary, short messages may have to wait for the link to transition for longer than the packet requires for transmission. This is detrimental to latency when the network is sparsely used, as is the case in most HPC environments. Moreover, during transitions, link power consumption is the same as when in the *Wake* state.

The IEEE 802.3az draft [32] specifies values for t_w and t_s for several Ethernet specifications, as shown in Table 2. For a comparison, the time to send a 1500-byte frame has also been considered. As we can see, higher speeds reduce frame times, but increase *Sleep* and *Wake* transition times considerably. Therefore, LPI is suitable for large bursts followed by large periods of inactivity.

Protocol	t_w	t_s	Frame time (1500B)
100Base-Tx (100 Mb/s)	30 μ s	100 μ s	120 μ s
1000Base-T (1 Gb/s)	16 μ s	182 μ s	12 μ s
10GBase-T (10 Gb/s)	448 μ s	288 μ s	1.2 μ s

Table 2: Link transition times for different Ethernet versions (extracted from [32]).

2.4. Energy Efficient Ethernet (EEE)

The IEEE 802.3az standard, also known as Energy Efficient Ethernet (EEE) [11, 32], makes use of the Low Power Idle (LPI) mechanism to reduce energy consumption during idle periods on Ethernet links. This mechanism defines two states: *Active* and *LPI*, which involve transitioning between normal operation and a low-power mode. The EEE standard specifies only the basic behavior of LPI, leaving implementation details such as transition policies to the vendors.

When EEE development started, only *Sleep* and *Wake* (sometimes referred to as *Idle* and *Active*, respectively) were envisioned to provide power savings. Later enhancements to the LPI mechanism were proposed in subsequent amendments to the IEEE 802.3 standard. Specifically, the IEEE 802.3bj amendment, which targets 40 Gb/s and higher-speed Ethernet links, introduces refinements such as the *Fast Wake* state [7]. Also, the former *Sleep* state is renamed as *Deep Sleep*. The *Fast Wake* state addresses the latency drawbacks of the original LPI proposal by maintaining partial activity in PHY components, while *Deep Sleep* shuts more components down. This reduces wake transition times significantly, from 4.6 μ s in *Deep Sleep* to around 250-500 ns in *Fast Wake*. However, this comes at the cost of reduced power savings, typically around 20–40% for *Fast Wake* compared to up to 90% in *Deep Sleep* [27]. Anyway, the criterion for designing transitions at the hardware is still left to the vendors.

Figure 3 illustrates how employing different low-power states affects link transition times and, consequently, the overall performance of data transmission in energy-aware systems.

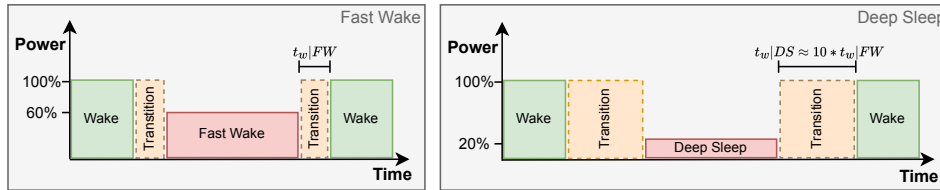


Figure 3: Visual representation of *Deep Sleep* and *Fast Wake* power states.

The different link power levels are a basis for implementing LPI, included in the EEE standard [11]. This has led to several proposals tailored for HPC so that end-to-end latency is not greatly increased by the overhead of turning links on [25, 4]. The idea for HPC environments is to employ Fast Wake so that latency is not greatly affected by ports powering up. However, transitioning up as soon as packet transmission ends causes ports to spend more time transitioning than transmitting packets. Table 3 shows a summary of the available states in EEE, with their link power and transition time.

State	Link power	Transition time to Wake
Wake	100 %	-
Fast Wake	60-80 %	250 - 500 ns
Deep Sleep	10 %	4.48 μ s

Table 3: Summary of EEE link power states (based on [7]).

2.5. Proposals to complement EEE

The main basis behind power management in interconnection networks is that link power consumption does not depend on usage. However, link usage is not constant because transmissions only occur when necessary. Moreover, the usage of any particular link is determined by several factors. For example, the traffic pattern, the topology, and the routing algorithm can have different effects on the usage of every link during the execution of an application. Deciding on when to switch to and from a power-saving state is important because the more power savings, the more overhead the link suffers.

The simplest power-saving strategy is to switch a port to a power-saving state as soon as a transmission is complete. When two connected ports have nothing to send, they can transition at the same time. However, switching to power-saving states for every transmission entails transitioning to the *Wake* state before the next transmission as well. Even during the most intense

communication periods, traffic is not sent at once, and link usage is recurrent and intermittent.

One option to reduce transitions is frame buffering: accumulating packets on buffers and only transitioning to *Wake* on certain conditions [11, 27]. Once a packet is on an output port buffer or is granted crossbar traversal on switches, an occupation threshold and a time limit are set. The buffer occupation is set to exploit packet coalescing and thus, avoid transitioning to *Wake* once per packet. However, a timeout is needed to ensure packets are eventually sent regardless of the buffer occupation. Obviously, this can cause additional latency for every hop. In the worst-case scenario, every communication is composed of small and spaced out packets that do not coincide in time or share network paths. This means that packets will be stalled at every port and have their latency increased both by the buffering timeout and the transition time to *Wake*. Of course, this is not viable for latency-sensitive applications. As we cannot assume packet coalescing to mitigate the overhead of port transitions, the only option left is to keep links in the *Wake* state for longer. If the port is left in *Wake* state for a moderate period after transmission, there is no overhead to a packet that must be transmitted within that time. Power Down Threshold (PDT) [27] was proposed so that every port stays operational for an additional time after transmission, at the cost of potential power saving.

A simple implementation of PDT can be done by using a timer on each port. The port switches to power-saving mode when the timer expires without transmitting a packet. If any packet arrives at the port, either from the link or via arbitration or fragmentation, the timer is canceled. It will be set again on the last port that has transmitted through the link, once it has no packets to send.

Figure 4 shows link behavior when using PDT in terms of power consumption over time. The blue arrows represent the duration of the timer used in PDT, and the colors of the timer icon represent changes in the timer used in PDT. The green-colored timer means that it is set, while the red indicates that the timer is canceled, and the salmon is for the timer expiration. We can see that during the *Wake* state, packets present at the port can be sent normally. After sending a packet, the port waits for a certain period (t_{PDT}) to transition to the *Sleep* state. If a packet arrives within t_{PDT} after sending a packet, the timer is canceled and set again when the packet is transmitted.

This way, ports that may frequently transmit will be in the *Wake* state most of the time, but packets will not suffer from latency because ports are

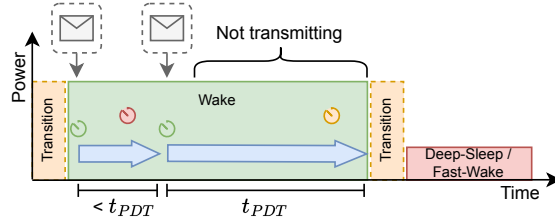


Figure 4: Diagram of LPI using PDT.

ready to send them. Meanwhile, for inactivity periods that are on the order of seconds, the overhead on latency for state transitioning is irrelevant. A t_{PDT} value of microseconds is also insignificant compared to the inactivity period in terms of power saving. The issue, as we have mentioned, is the intermittent nature of network activity during communication. When the t_{PDT} is on the same order of magnitude as the inactivity periods, ports may often receive packets after powering down, or even while transitioning.

The main inconvenience of the PDT technique is the criteria for choosing a value and its generalization to all network ports. The former depends on the application and would require prior execution for inactivity profiling. This would be useful if the inactivity periods of the ports could be estimated beforehand. However, they depend on multiple factors, such as task mapping and the number of processors on the nodes, which affect the traffic pattern. In a production environment, the values would have to be set depending on the application. The latter issue of PDT is that inactivity periods differ between all ports. This can be caused by network topology or task scheduling. The topology determines the average and maximum hop count for packets between a source and destination, both by the layout of network elements and the routing algorithm. In fact, the higher the hop count, the larger the overhead due to port transitions.

Due to these limitations, ports should establish their own t_{PDT} value, based on previous network activity. To solve this issue, Saravanan proposed PerfBound [28]. The basis of PerfBound is forming a histogram on each port with the inactivity periods so that port can calculate its particular t_{PDT} at any given moment in a way that degradation is bound. PerfBound also requires every port to store (or calculate) the distance in hops of any packet, given a destination. It uses one counter per possible distance value to calculate the average distance of previous packets. In this way, we can quantify the possible degradation of a packet due to the powering up of multiple ports along its route.

To calculate the next t_{PDT} value, the algorithm first determines the number of packets that can be delayed due to power-up transitions within a given degradation limit. For example, if we want to maintain a performance degradation restriction of up to 1 % in a period of duration X , we can delay up to $N = 0.01 * X/t_w$ packets, where t_w is the transition time to *Wake*. We use the average distance to destinations described earlier as a corrective factor l for each port. By doing so, we are less restrictive on ports with higher mean distance. In a generalized manner, $l = (bound\%) \times \sum_{i=1}^n \frac{p_i}{h_i}$, where n is the number of different hop counts, p_i is the proportion of packets that travel h_i hops and h_i is the number of hops for the i -th group of packets.

For example, if 60 % of packets sent by a port are 6 hops away from the destination, and the distance for the remaining 40 % is 4 hops, we would calculate that factor for a 1 % degradation threshold as in Eq. 1:

$$l = 0.6 \times \frac{0.01}{4} + 0.4 \times \frac{0.01}{6} = 0.01 \times \left(\frac{0.6}{4} + \frac{0.4}{6} \right) \approx 0.0022 \quad (1)$$

To apply this factor, the new number of packets will be $N = l * X/t_w$. Once we have obtained N , we search on the histogram, from highest to lowest bin, and accumulate the count of each bin. We are looking for the leftmost bin that accumulates at most N . We will set the t_{PDT} to the mean of that bin.

2.6. BXIv3 network technology

BXIv3 [15] is the network technology being developed by Eviden for HPC systems and data centers. The main objective for Eviden is to develop an interconnect that can power post-exascale systems. The existing versions of BXI, namely V1.2 [12] and V2 [6], are already deployed in several TOP500 supercomputers, including CEA-HF and Tera-1000-2 [35]. Choosing Ethernet as a basis means that there is a grounded work on standards that can speed up the development of the technology. Some examples of this set of standards are the 802.1Qbb or priority flow control (PFC) [39] for lossless per-queue link-level flow control, or the possibility to use variable-sized packets and jumbo frames.

BXIv3 network interfaces (NICs) support a link bandwidth of 400 Gbps (expected to be 800 Gbps in the near future), with a target deployment scale of up to 100,000 nodes, following the modular supercomputing architecture (MSA) specification [33]. BXIv3 supports different network topologies, such as Fat-trees and Megaflly/Dragonfly+ [16, 31], which permit the desired levels

of interconnection scalability. BXIV3 switches assume a Combined Input-Output Queued (CIOQ) switch architecture, similar to other Ethernet-based options. Regarding power consumption, we are not aware of any proposal tailored to BXIV3². We believe that, given the high consideration for power consumption, it will be a cornerstone for future interconnection technologies.

3. Power consumption model

This section describes the interconnection network power model tailored to the BXIV3 architecture we implemented in our network simulator. This model is based on the Energy Efficient Ethernet (EEE) standard (see Section 2.4 and the extensions proposed to expand its functionality (see Section 2.5), such as LPI, PDT, and *Perfbound*). We have also designed some improvements to the *Perfbound* strategy, so that EEE can be better applied to Ethernet-based interconnection networks when used to run HPC applications.

The EEE standard specifies the PHY layer behavior, but the transition between link states is left to the vendor. For BXIV3-based interconnection networks, we assume a combined input-output queued (CIOQ) switch architecture. Specifically, BXIV3-based switches define buffers at input and output ports, so it is possible to grant switch crossing requests from input buffers to non-operative ports, i.e., to output ports in the *Sleep* state. This way, packets will be stored on their respective output queues when ports power up, i.e., when returning to the *Wake* state.

We have opted to implement and experiment with the EEE standard because BXIV3 and further switch generations are Ethernet-based³. Furthermore, Eviden, the French company devising BXI, is one of the founder members of the Ultra Ethernet Consortium (UEC), where Eviden has planned a Roadmap for BXIV4 and BXIV5 generations in this decade. Since the UEC explicitly aims to scale relatively flat Ethernet networks to support up to 1 million endpoints within the next several years, the power management will be a cornerstone to keep proportional energy consumption in these networks.

In the following sections, we describe the EEE-based power model details regarding link power states, transition logic using PDT, implementation of

²Further details on the BXIV3 architecture can be obtained from one of the papers describing the BXIV3 architecture in the RED-SEA project [14].

³<https://tinyurl.com/a484fjpj>

Perfbound, and the improvements made to adapt these techniques to BXIV3 networks when running HPC applications.

3.1. Link power-levels and transition logic

The link power levels are as described in the EEE standard, with three states: *Wake*, *Fast Wake*, and *Deep Sleep*, and as we showed in Table 3. As the EEE only specifies the components to shut down and the corresponding timings to transit between them, it is also up to the vendors and network architects to decide when and how to switch states.

Our proposal for deciding on port state transition revolves around the state of the output queues. This way, ports that have sent packets will notify their remote ports to power down, synchronizing their transition.

Figure 5 shows the request-response mechanism that two ports from different devices, connected by a link, use to change states at the same time. At T_0 , port A requests synchronization to either power up or down. Port B receives the request at T_1 , and responds at T_2 with the answer. Port A has not only the response, but can also calculate the Round-Trip-Time (RTT) to establish the start of the transition, marked in the figure at ‘Sync’. Port A sends a message to signal the end of synchronization so that Port B can also calculate the RTT.

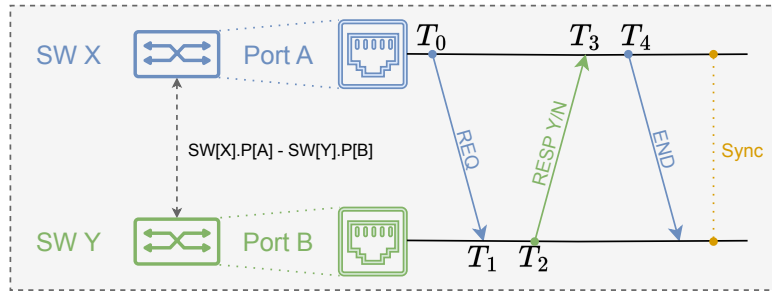


Figure 5: Port state synchronization between two switch ports.

The criterion to accept or refuse to transition mainly depends on the port buffer occupancy. When a port is requested to power up, the response is always positive and the port switches to the *Wake* state. Upon receiving a power-down request, a port responds with a rejection if its output buffer is empty, or with an ongoing transmission that the remote port may not be aware of. Otherwise, it responds affirmatively, and both ports synchronize

to start the transition to the *Sleep* state. This message exchange provides an insignificant overload: a 64-byte message encoding these messages requires 1.28 ns at 400 Gbps, which results in a delay below 5 ns in the case of a negative response to power down before the consequent packet transmission.

An output port in the *Sleep* state may request to power up when it receives a packet from an input port via switch arbitration. In fact, it is the only way to trigger it because the remote input port at the next switch is also powered down. A control message is sent over the link to ensure the remote port transitions simultaneously, and the packet flowing over the link connecting these two switches is restored. By contrast, if an output port is transitioning to power down and receives a packet via arbitration, it must start powering up as soon as it ends its transition down; otherwise, the synchronization between the two sides of the link becomes more complex.

The PDT timer at a given switch port should always be set when a link is transmitting and expire only after all data has been sent from that port. In other words, expiration would mean that a port has already transferred all of its data. Therefore, when a port receives a packet in its output buffer, it resets the PDT timer to start counting after the packet is fully transmitted. The other port cancels the timer upon reception. This way, the last port transmitting is the one that ultimately requests to power down.

3.2. *PerfBound* implementation details

While *PerfBound* provides grounded methods to trade power saving for performance, some implementation and evaluation aspects are set under the authors' discretion.

For example, the histogram formed of inactivity period lengths is the key piece of the mechanism. However, even if clearing the histogram (or *refreshing*, as the authors mention) is pondered, its consequences are only theoretically mentioned. There may be several possibilities for managing the histogram to constrain its storage size and maintain a bias towards recent values.

Another important aspect of the algorithm is using average hop distances from switches and nodes to destination nodes. The experiments exploring the original work set a constant hop count for the network. However, this is non-realistic and may be affected by the traffic patterns of different applications. Devices should have their own record of hop distances, based on the destinations that can be reached according to their routing algorithm. Distance calculations depend on the topology and routing employed, and should be

straightforward on regular topologies. On irregular topologies, however, hop distances should be calculated beforehand. Employing routing information may also decrease the effectivity of the algorithm if the routing algorithm is adaptive and hop counts change depending on the network status.

Another important aspect of PerfBound is that, while it provides a sensible approximation to a useful t_{PDT} value, the final execution time overhead is unknown beforehand. For example, if we have an application that completes its execution in 100 seconds and we set PerfBound to only allow 1 % overhead, the maximum possible overhead should be 1 second. During the execution, we will have multiple calculations for t_{PDT} values on every port, and we will necessarily miss some predictions, degrading performance. The target overhead can be reached or surpassed during the application execution, but we have no way to notice (we assume we do not know the execution time beforehand). More importantly, the overhead is purely additive. Therefore, even if we could track the overhead during execution, we could not overcompensate for the threshold having been surpassed.

The recurrent calculation of a PDT timer expiration value for every port is also concerning. More so for switches, which would need to do so every time all output queues for any port are emptied. We believe that this processing should be carried out on a regular basis, but only if there was network activity on a port since the last calculation.

3.3. Additional requirements

All network equipment already has the circuitry and mechanisms to implement the different power-saving states defined in the EEE standard. However, vendors must define the logic to switch between port power states.

Using PDT requires, per port, one timer and a separate register to store the configured t_{PDT} . The time resolution and maximum possible value are determining factors. For instance, a 32-bit unsigned register with up to nanosecond precision can encode $2^{32} * \frac{1s}{10^9ns} \approx 4.295$ seconds. Table 4 shows the maximum time that could be encoded in a register with several register widths and various time resolutions.

For PerfBound, each port requires storage to form the histogram. The most naive implementation would be storing each inactivity duration in a sorted list to facilitate the calculi of the next t_{PDT} value. However, it would be more feasible to set a constant bin width and store bin counts instead, at the cost of precision. An improvement on this would be to use a map-based structure instead. This way, recurrent bins do not increase storage size. As

		Resolution			
		1 ns	10 ns	100 ns	1 μ s
Width	16 bits	66 s	655 s	7 ms	66 ms
	32 bits	4.3 s	43 s	429 s	4×10^3 s
	48 bits	2.81×10^5 s	3×10^6 s	28×10^6 s	2.81×10^8 s
	64 bits	1.8×10^{10} s	1.84×10^{11} s	2×10^{12} s	1.8×10^{13} s
	128 bits	3.4×10^{29} s	3×10^{30} s	3.4×10^{31} s	3.4×10^{32} s

Table 4: Maximum time values to encode with several time resolutions on multiple register widths.

we are storing bin indices instead of raw time differences, the width does not have to coincide with that of the t_{PDT} .

With finite memory, regular clean-up of the recorded inactive periods should be carried on. If the histogram is cleared every N elements collected, a possible storage solution is a FIFO queue with at most N bin indices. Then, the histogram can be formed by the elements in the queue. Alternatively, only the oldest element can be removed if the histogram is cleared periodically without any other concern, and the size is indefinite. However, steep memory requirement increases are not expected if cleared within a sensible period, like one second, at most. Moreover, the packet rate and size to cause this would be extremely inefficient because a significant part of the traffic would be the overload from packet headers. And even then, those inactive periods would fall under a few bins. Ultimately, the space required to store inactivity periods is determined by bin width (w_{bin}) and the highest possible bin (max_{bin}), with up to max_{bin}/w_{bin} total counts. If the histogram is cleared every TTL_{hist} seconds, it cannot have more than TTL_{hist}/w_{bin} different bins. If the decision to clear the histogram is based on the number of values collected, the largest histogram would be one of N bins with count 1.

3.4. Improvements to Perfbound: PerfBoundCorrect

Even if PerfBound is a grounded basis for predicting a reasonable t_{PDT} value, it presents mainly two drawbacks. The first one is that collecting previous values to calculate a new t_{PDT} is ultimately a prediction of a concrete value. Prediction is widely used in decision-making on computers, from branching predictors to unattended maintenance at low-impact intervals.

However, missing predictions often have no more performance penalties than the overheads obtained by not using the predictor. But this is not the case for PerfBound, and the performance impact of every missed prediction

is quantifiable. We can calculate the ratio between a period of inactivity that caused a port to power down and the last t_{PDT} value. That proportion can help quantify the error factor in missed predictions. If we collect several of these values, we can calculate a corrective factor to increase the t_{PDT} value according to the missing rate and ratios. We call this technique *PerfBoundCorrect*.

We need a shift register and a queue containing the last ratios to track the last predictions. Every time a packet arrives at a port, if the PDT is still set (the port is up), we count this as a hit, or a miss otherwise. We can store this history in a shift register of length n_R . When a port starts its transition to power up, the ratio is calculated and stored in a FIFO queue of length n_R at the same time as the shift register is updated. If we remove a miss from the register by shifting, we also have to pop the oldest element from the queue. This way, we keep as many elements on the queue as misses encoded at the shift register. The proportion between the miss count and the shift register length returns the hit rate of the last n_R predictions, and the queue of ratios can be used to get a correcting factor. It is important to note that a greater ratio of outliers is expected and reasonable, since they appear when a long inactivity period has finished. In those cases, the overhead of transitions is acceptable because they are the best opportunities for power saving.

To apply the correcting factor to the PerfBound calculation, we have opted for the geometric mean of all ratios times the miss rate for the last T_{PDT} value. The geometric mean was chosen because it is more tolerant of outliers than the arithmetic mean. The corrective factor (cf) applied to the t_{PDT} calculation is as follows:

$$cf = miss\% \times \left(\prod_{i=1}^n x_i \right)^{\frac{1}{n}} = miss\% \times \sqrt[n]{r_1 r_2 \cdots r_n}$$

To prevent too small cf values and result in unreasonably high (i.e., second range or above) t_{PDT} values, we set a maximum limit $max_{t_{PDT}}$ within a sensible order of magnitude. The corrective factor cf_b will be $min(cf, max_{t_{PDT}})$. Giving this leeway to the PerfBound algorithm may seem harmful to power saving as links would spend more time operational after their transmissions end. However, it also has the potential to reduce the overhead caused by very reduced t_{PDT} values. This is our proposal, and the results are non-trivial, as we will see in Section 4.

4. Evaluation

In this section, we will evaluate the mechanisms previously proposed, which we have implemented in SAURON [37], our OmNet-based network simulator. Using this simulator, we have prepared some experiments to test power-saving strategies. Regarding the network traffic, our simulator employs the VEF-TraceLib [2, 3, 5] library to inject traces from real applications into the simulator. TraceLib also provides us with a statistic of CPU usage, which will help us model the dynamic CPU usage-to-power conversion. We assume that the power consumption for nodes is mostly determined by the CPU, whose power is a direct function of usage, with a minimum power draw at idle. We also use the TopGen [36] library and its file generator to model large-scale networks with multiple topologies.

The scenario we have chosen for the experiments is a Megafly [16] topology composed of 4160 computing nodes. The network is arranged in 65 groups of 64 nodes, each group employing 16 switches with a radix of 16 (1040 switches in total). The inter-group connectivity is as described in the original Megafly publication, with one global link containing every pair of groups. Our decision on this topology is its scalability, flexibility, and popularity in HPC environments [23]. This topology can exploit the relative locality of nodes located in the same group for fast efficient communication in disjoint network partitions that exchange their messages through high-bandwidth global channels. This node arrangement can help perform partial calculations in the same-group nodes and use the global links for reductions. AI workloads, and most recently, Large Language Models (LLMs), can also benefit from this topology, as several kinds of parallelization employ different broadcast domains. Compared to the Dragonfly, the main advantages are the use of low-radix switches and the inherent absence of deadlocks. The routing algorithm employed is deterministic and minimal. When a packet has its source and destination in the same group, the algorithm behaves like D-mod-k [38]. However, when the destination is in another group, the packet travels to the spine switch that will lead to the destination group through a global link. When the packet arrives at the destination group, the downward path is the same as in D-mod-k, with only one possible route.

Table 5 shows the power consumption of the different elements that make up the whole system. These figures are based on information on modern server processors and expected network power draw provided by Eviden. The asterisk on minimum link power consumption depends on the different

power-saving states that are employed. The total link number accounts for the link on every switch times the radix, with the addition of every NIC. The system is considered idle when the nodes are not doing any computation and thus, consuming their minimum power. Switch power only comprises the device power draw with no links connected.

Element	Power/Unit		Count	Power (all)	
	Min	Max		Min	Max
Switch	250 W	250 W	1040	260 KW	260 KW
Node	800 W	1200 W	4160	3.328 MW	4.992 MW
Link	*	24 W	20800	*	499.2 KW
				*	5.751 MW

Table 5: Power consumption of the different components of the system.

On the contrary, under full load, the system consumes approximately 3.788 MW. In both cases, the contribution to power consumption by the network is the power consumption of switches and links, 260 KW and 124.8 KW, respectively, adding up to 759.2 KW. In proportion, the network accounts for 12.214 % of power when the system is idling, and up to 8.68 % under full load when all nodes are computing. A way to save power on links is to employ the EEE standard and its power-saving link states.

In Table 6, we define the power parameters for each power-saving state, such as the power reduction and the time to transition from the power-saving state to the active state (t_w), and its counterpart (t_s), derived from EEE (which we showed in Table 3). The table also shows the percentage of power that the system devotes to the network upon applying those values to our selected scenario. The calculi for the power contribution of different elements is similar to the one by [4].

For the evaluation, we have selected traces of two HPC applications (LAMMPS, PATMOS) and two distributed Deep Learning training sessions (MLWF [22] and AlexNet [21]) to study the network behavior in both contexts. For each application, we will first describe the behavior of the ap-

Port power state	Power	t_w	t_s	Network/total power		Links/network power	
				Idle	Full load	Idle	Full load
Wake	24 W	-	-	18.575 %	13.201 %	12.214 %	8.68 %
Fast Wake	9.6 W	375 ns	200 ns	12.136 %	8.432 %	5.272 %	8.68 %
Deep Sleep	2.4 W	4.48 μ s	2 μ s	8.519 %	5.845 %	1.372 %	8.68 %

Table 6: Network contribution to total system power consumption across two scenarios.

plication and the potential for energy saving. First, we will compare how much energy we save with different techniques in comparison to not using any power-saving technique. Non-energy metrics include the degradation that is introduced by power-saving strategies. Mainly, we want to focus on the increase in execution time and latency. Specifically, the latency metric we are exploring is the packet latency, which measures the time from the packet generation to its arrival at the destination.

In the tests where a fixed PDT is employed, we have tested 9 possible t_{PDT} values, from 0 to one second. For PerfBound and PerfBoundCorrect tests, we have tested 3 degradation thresholds (1, 2, and 5 %) on each of the histogram types we discussed in section 3.2.

4.1. Evaluation for the LAMMPS application

The LAMMPS molecular dynamics uses the network to exploit its parallel architecture and keeps the model distributed among nodes. The simulation space is divided into subdomains assigned to different processors, each of which manages *own atoms* and *ghost atoms*—copies of neighboring atoms needed to calculate interactions.

To maintain synchronization across subdomains, LAMMPS relies heavily on MPI communication, which generates traffic in two main forms. Point-to-point (P2P) messages are used to transfer data between neighboring subdomains for short-range interactions. LAMMPS also uses several collective communication operations: `MPI_AllReduce` (which dominates overall communication and can lead to network congestion) aggregates data across all processors; `MPI_Broadcast` distributes control information; and `MPI_AlltoAll` is used during FFT computations for long-range interactions, adding to the global traffic.

In summary, LAMMPS creates a mix of localized and global communication patterns, with `MPI_AllReduce` identified as the primary contributor to potential network bottlenecks, especially in large-scale simulations. Being an all-to-all communication operation, `MPI_AllReduce` will use most paths between nodes. This means that this operation will have the most degradation if all links are in a power-saving state. Figure 6 shows the network efficiency or throughput (normalized against the total network bandwidth) for the complete execution time (2.431 seconds) in the configured system. The total energy consumed is 9.993 MJ by nodes and 1.846 MJ by the network, totaling 11.839 MJ for the whole system. We can see that after a

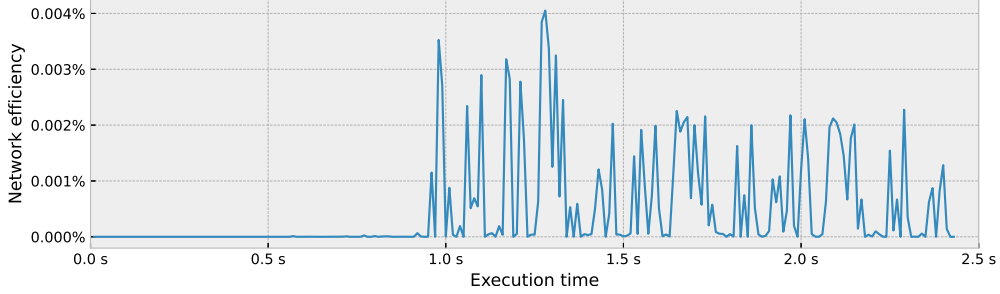


Figure 6: Network efficiency for the LAMMPS application.

second of computation, the network activity starts being intermittent with several traffic spikes due to the inter-node collective operations.

4.1.1. Results with fixed t_{PDT} values

The first statistic we will examine is the execution time, displayed in Figure 7a. We can see that using Deep Sleep causes the execution time to go beyond 100 %, while Fast Wake never surpasses 10 % overhead with t_{PDT} values below 10 μ s. This coincides with the t_w for Deep Sleep being an order of magnitude above that of Fast Wake. We can see the overhead drops significantly if a t_{PDT} of 100 μ s or higher is chosen, as this interval surpasses the length for most of the inactivity periods.

Figure 7 shows the impact of different t_{PDT} values on execution time, energy savings, and packet latency for LAMMPS. As we can see in Figure 7b, Deep Sleep achieves negative power consumption reduction when using 10 μ s and below, in accordance with the increment in execution time shown in Figure 7a. We can also see that using Fast Wake produces an increment of power consumption with t_{PDT} below 1 μ s, but it achieves energy savings close to 10% with t_{PDT} values larger than 10 μ s. In this latter case, Fast Wake obtains an overhead in the execution time of less than 10%. With more permissive t_{PDT} values, Deep Sleep produces more power savings.

If we look at the packet latency overhead in Figure 7c, we can see that the tendency for each t_{PDT} value is similar to that of the execution time, albeit on another order of magnitude.

In general, when using a fixed t_{PDT} value, we can see that the maximum energy savings are close to 10% when a LAMMPS application is run using our power model and the t_{PDT} values are higher than or equal to 100 μ s. With this t_{PDT} , the overheads in execution time and latency are also negligible. Fast Wake is more sensitive to smaller t_{PDT} values and achieves better energy

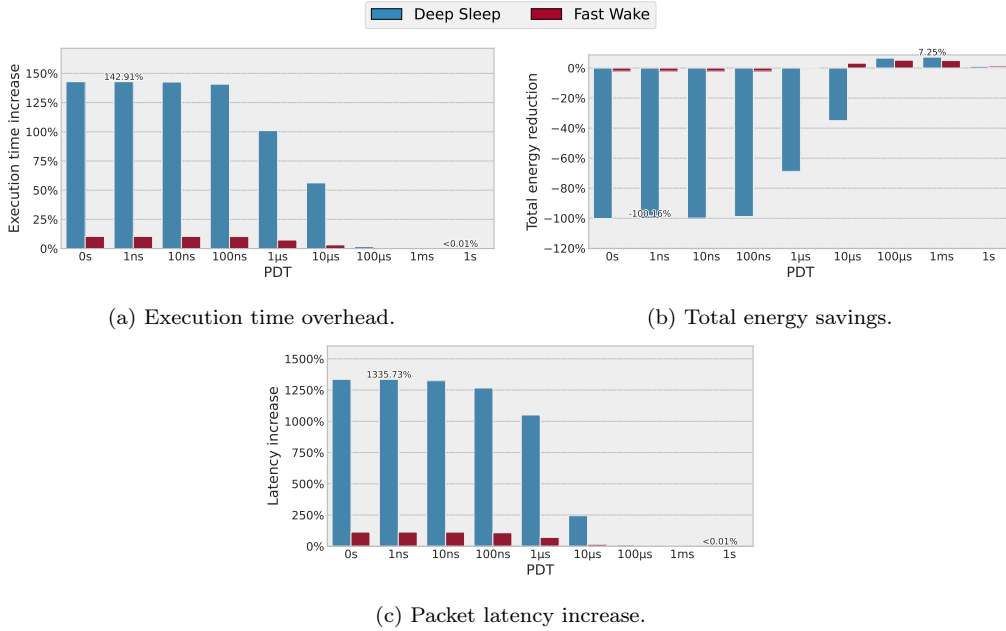


Figure 7: Impact of different t_{PDT} values for LAMMPS.

savings with smaller t_{PDT} values. Finally, note that with fixed t_{PDT} values larger than 1ms there are barely energy savings.

4.1.2. Results using PerfBound and PerfBoundCorrect

As shown in Figure 8a, we can see the overhead on the application when using PerfBound and PerfBoundCorrect techniques. Just like with a fixed t_{PDT} , the difference between Fast Wake and Deep Sleep remains in the same proportion. It is important to note that using either of the histogram types makes a negligible difference in the case of Fast Wake, but has an effect when using Deep Sleep. Using a circular buffer to store the inactivity periods provides the worst results by a noticeable margin. We can also see that clearing the histogram instead of replacing old records is better for the execution time, likely because values become more permissive each time the histogram is reset. Recording all the inactivity periods provides a lower execution time overhead. However, the advantage of the self-clearing histogram comes at the cost of storing an indefinite number of bins, which is not feasible.

We must also point out that even if PerfBound thresholds affect the calculi of every t_{PDT} value throughout the simulation, their impact on the end

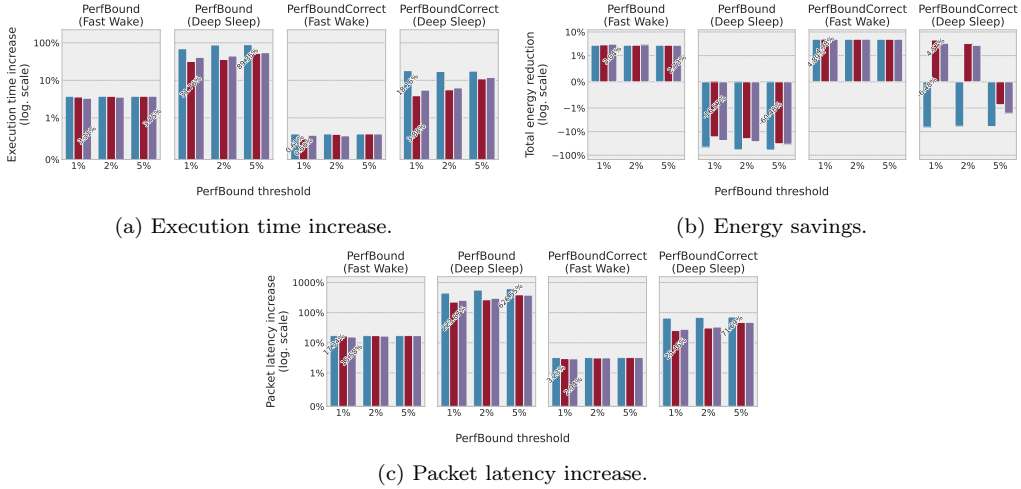


Figure 8: Impact of PerfBound and PerfBoundCorrect on the LAMMPS trace.

result is not as straightforward as the original work suggests. Firstly, the calculations of t_{PDT} are heavily dependent on the previous history. This poses a problem when the history record is forming, and is sensitive to irregularities and fluctuations in timings. Moreover, we cannot assume that the whole system is being used for our application. Any other traffic can disturb the formation of our records and thus, future t_{PDT} values if deployed.

The overhead on execution time has a direct impact on the energy consumed, as seen in Figure 8b. Both PerfBound and PerfBoundCorrect provide similar levels of energy savings, with slightly higher values using PerfBoundCorrect. While PerfBound with Deep Sleep does not lead to energy savings, for thresholds of 1 % and 2 % PerfBoundCorrect manages to revert that situation. When using a high threshold, however, energy saving does not occur because the calculated t_{PDT} values are too short.

Finally, Figure 8c shows that PerfBoundCorrect, in all cases and with either power-saving state, reduces latency significantly. It is clear that, particularly when using Deep Sleep, a circular buffer to control the size of the histogram produces the highest overhead.

We must also point out that even if PerfBound thresholds affect the calculi of every t_{PDT} value throughout the simulation, their impact on the end result is not as straightforward as the original work suggests. Firstly, the calculations of t_{PDT} are heavily dependent on the previous history. This poses a problem when the history record is forming, and is sensitive to irregularities

and fluctuations in timings. Moreover, we cannot assume that the whole system is being used for our application. Any other traffic can disturb the formation of our records and thus, future t_{PDT} values if deployed.

4.2. Evaluation for the PATMOS application

PATMOS [9] is a Monte Carlo neutron transport code developed at the CEA (France), designed to prototype applications in nuclear safety and radiation shielding.

To facilitate statistical analysis, simulations in PATMOS are organized into batches, even though source particles are independent. For example, one million particle histories might be simulated as 1000 batches of 1000 particles each. This batching approach allows for robust estimation of confidence intervals, as the averaged batch tally values tend to follow a normal distribution.

During each simulation cycle, particles are evenly distributed among threads, with each thread responsible for simulating particle histories and updating the associated scores. By default, a static scheduling is used so that the parallelization strategy is deterministic, ensuring reproducibility and simplifying debugging.

When using MPI for distributed simulations, each MPI process independently runs a full, standalone simulation. Upon completion, results are aggregated using collective MPI operations: `MPI_AllReduce` is used to compute the global mean, followed by `MPI_Reduce` for variance calculation.

This last description coincides with the evolution of network efficiency shown in Figure 9. As we can see, the application only accesses the network during startup and upon completion. The rest of the time, as nodes are executing independent simulations, is an opportunity for power saving on the network. With no power-saving strategy on links, the application execution time is 1290.64 seconds. During that time, the whole system consumed 7.334 GJ, operating at 5.685 MW, very close to maximum cluster capacity. The network has consumed 345.28 KJ. In terms of efficiency, the whole system is at 8,75E mJ/bit, and the network is at 412,08 nJ/bit.

4.2.1. Results with fixed t_{PDT} values

The first statistic we will analyze is the execution time, as it is the one that is most noticeable in terms of overhead, and a longer execution times have a negative impact on total energy consumption. In our experiments, applying any power-saving technique did not affect this application. The reason behind

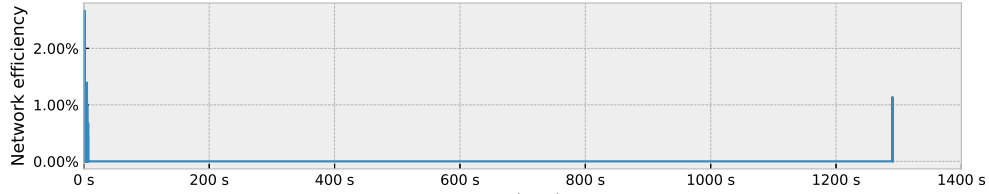
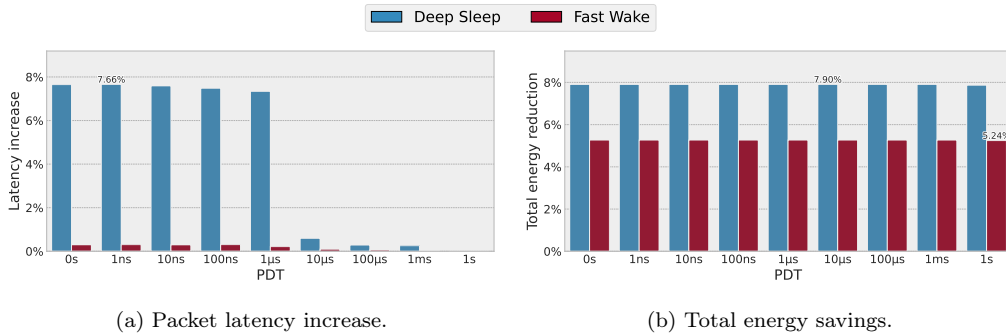


Figure 9: Network efficiency for the PATMOS application.

this is that performance overhead is cumulative with the number of packets that get stalled on output ports. Therefore, as the network is only used at the start and end of the simulation, the effect on execution time is virtually non-existent.

The other possible overhead for the trace is related to latency. If we look at Figure 10a, we can see the effect each t_{PDT} value has on packet latency. As we can see, employing Deep Sleep increases the packet latency by up to 7.5 %, with a step increase on the microsecond scale and below.



(a) Packet latency increase.

(b) Total energy savings.

Figure 10: Impact of different t_{PDT} values for PATMOS.

Regarding the total energy consumed, leaving links operational after transmission is potentially beneficial for future outgoing packets at the cost of more energy consumed over time. Figure 10b shows the effect each PDT value has on the total energy consumed by the system. As is the case with execution time, the ports experience few transitions because of the traffic pattern of the application. As such, the energy saved on links is very high, with ports being, on average, on for only 0.02 % of the time.

4.2.2. Results using PerfBound and PerfBoundCorrect

The execution time with any fixed t_{PDT} value is nearly identical to the configuration to not applying any power-saving. PerfBound, focusing on

minimizing the overhead on execution time, is no exception. Every execution time with any threshold or histogram management scheme yields the same results.

Latency results show a minimal increase, as shown in Figure 11a. Deep Sleep, having a t_w value an order of magnitude above that of Fast Wake, causes its latency overhead to be also higher. If we look into the different histogram strategies, we can see that having a regular histogram provides the lowest overhead of the three, no matter the PerfBound threshold chosen. This is because abnormally high values on the histogram cause the algorithm to find a suitable value early on, thus resulting in high t_{PDT} values. The self-clearing histogram resets itself after 250 values collected, which will statistically remove more small values than large ones, thus resulting in more permissive t_{PDT} values. And lastly, the histogram with a circular buffer, having only the latest values, has a heavy recency bias. However, all the ratios in the histogram count the same towards the geometric mean, no matter how new they are. As such, in periods where network inactivity is increasing, the predictions start to miss more often, resulting in more overhead.

When using PerfBoundCorrect, we can see that when using Deep Sleep, the latency overhead has been reduced to a third compared to PerfBound, and halved in the case of Fast Wake. We can see that the overall relation between the different histogram kinds is the same as it was with the regular PerfBound, and it is reduced in a similar proportion.

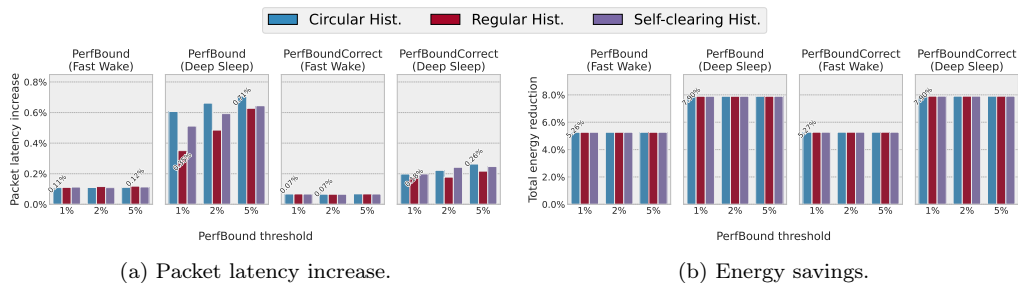


Figure 11: Impact of PerfBound and PerfBoundCorrect on the PATMOS trace.

If we look at Figure 11b, we can see the total energy savings on the system due to applying the power-saving techniques on the network links. We can see that for this application, there is no relevant difference in using one histogram type over the other, but using Deep Sleep yields greater energy savings. As expected in a situation with links having few and long inactivity

periods, Deep Sleep provides better power saving than Fast Wake.

4.3. Evaluation for the MLWF application

The MLWF (Machine Learning Weather Forecast) [22] application is developed within the context of the MAELSTROM European project. The trace was collected during a training session using Horovod [29]. The traffic pattern in this application, in particular, and in Deep Learning training sessions in general, usually involves the usage of MPI collective operations for data exchange. Particularly, the most predominant traffic portion comes from `AllReduce` operations. Usually, every layer of the neural network that is being trained runs a repetitive sequence of `Gather-Gatherv-Broadcast-Broadcast` until the weights converge, then the `AllReduce` is invoked to have the information on every node [5].

The network efficiency results for this trace are shown in Figure 12. We have opted to show them on a logarithmic scale to illustrate that any traffic rate, regardless of the value, provides great difficulty in finding opportunities for power saving.

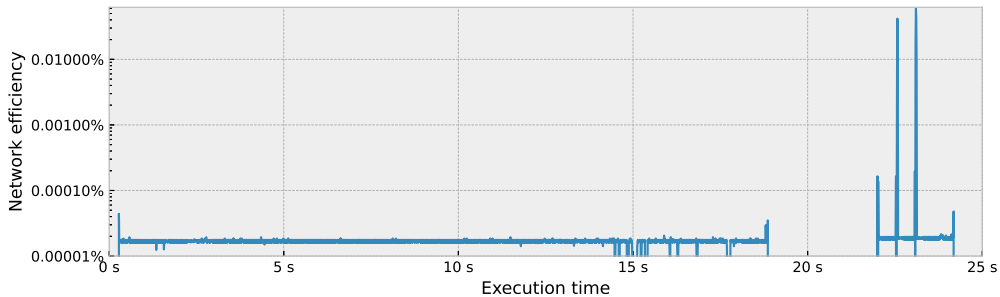


Figure 12: Network efficiency for the MLWF application.

4.3.1. Results with fixed t_{PDT} values

Figure 13a shows the increase in execution time for the application on different experiments. We can see that for small t_{PST} values, the overhead is in consonance with the t_w values for Deep Sleep and Fast Wake. To halve worst-case execution time overhead using Deep Sleep, we would have to set a t_{PDT} value above 1 μ s, and another 3 orders of magnitude to reduce it to a third.

As shown in Figure 13b, we can see that there is an evident difference between the latency overhead that occurs with either power-saving state. As

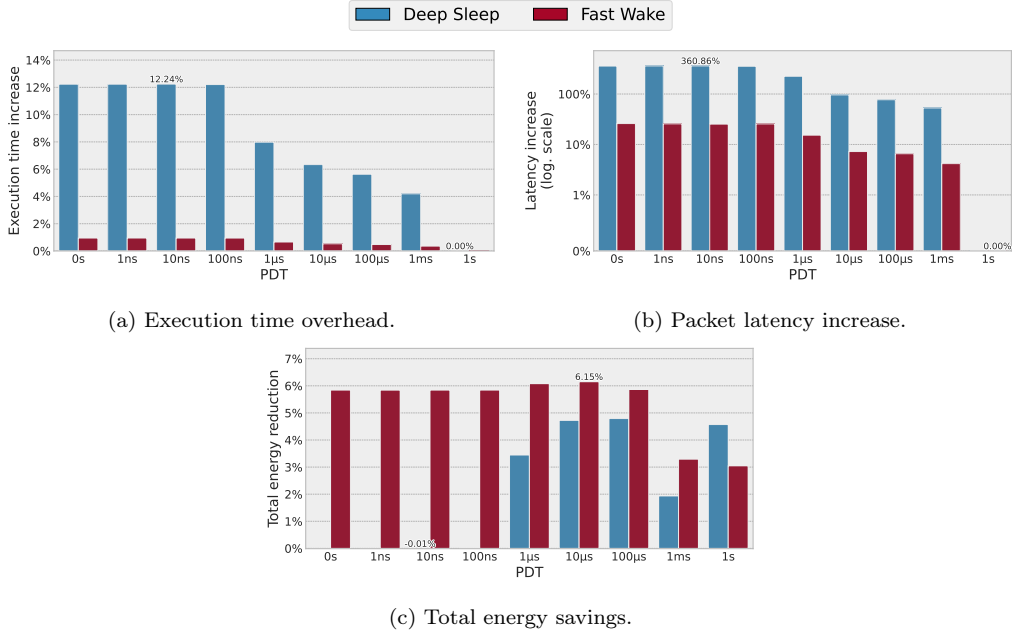


Figure 13: Impact of different t_{PDT} values for MLWF.

we increase t_{PDT} values, the latency starts dropping to lower, more acceptable values.

The results for energy saving for this application are shown in Figure 13c. As shown, t_{PDT} values of 10 and 100 μ s increase the energy saved in both power-saving states. Lower values provide marginal power-saving values or even increased energy usage in that proportion. Indeed, even if the traffic between the large bursts at the start and end of the applications, there is communication that is not negligible for us. However, once we use higher values, the energy reduction begins to diminish. This is due to inactivity, 99 % of periods being within the millisecond range. This is also the reason why using a 1-second t_{PDT} provides more power saving than a millisecond-scale one.

4.3.2. Results using PerfBound and PerfBoundCorrect

Figure 14a shows the overhead on execution time when using PerfBound and PerfBoundCorrect with either power-saving state on links. We can see that using Fast Wake impacts the execution time by less than 1 %, while the overhead is higher on Deep Sleep, due to its t_w value. Still, we can see that

PerfBoundCorrect reduces the overhead compared to PerfBound.

Regarding energy savings results displayed in Figure 14b, we can see that for this application, PerfBoundCorrect provides around 2 % less energy savings than PerfBound when employing Deep Sleep, and a smaller difference on the Fast Wake experiments. The results for energy consumed show similar trends as those for execution time (Figure 14a), meaning that for this application, having more permissive t_{PDT} values simply increments the time that links are on. This is because PerfBound already hits most of its predictions.

The packet latency results are shown in Figure 14c. We can see that for both Deep Sleep and Fast Wake, the overhead is very small. This further proves that PerfBound already makes good predictions, and PerfBoundCorrect produces diminishing returns.

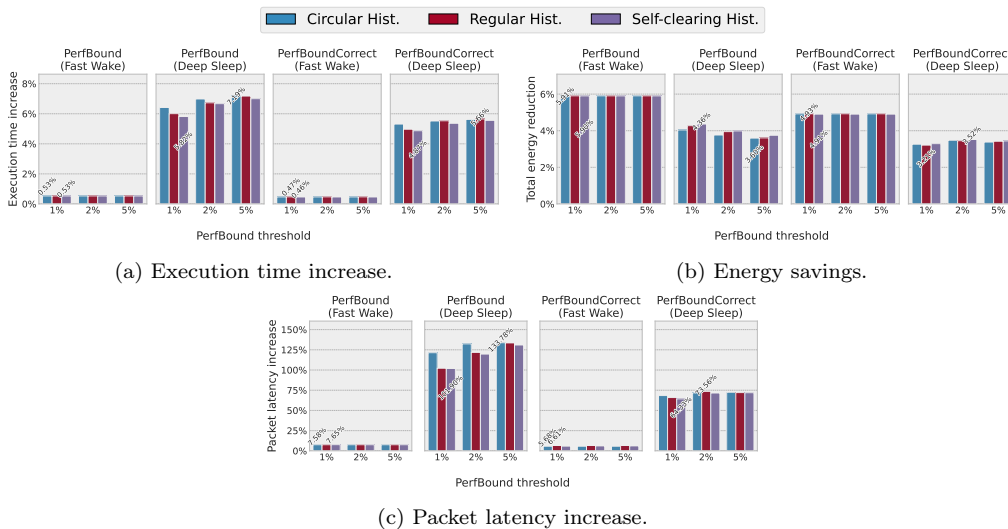


Figure 14: Impact of PerfBound and PerfBoundCorrect on the MLWF trace.

4.4. Evaluation for the AlexNet application

Our AlexNet traffic pattern is extracted from a training session, and it is shown in Figure 15. During this time, the main collective communications happen mainly during the back-propagation after each layer has been trained, and gradients are averaged by means of an AllReduce operation. We can see that the network is mostly idling, but there are periodic traffic bursts due to the collective communications. During the computation-heavy periods, however, we have opportunities for power-saving. Without any power-saving

applied, the system consumed 397.437 MJ in total, of which 323.786 MJ (81.469 %) are consumed by the nodes, and the rest comes from the network.

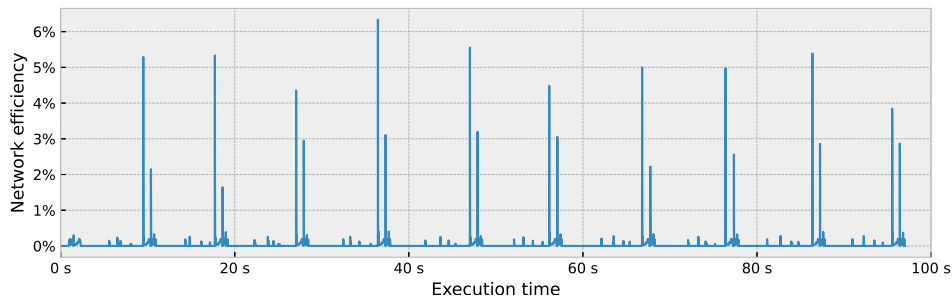


Figure 15: Network efficiency for the ALEXNET application.

4.4.1. Results with fixed t_{PDT} values

Figure 16a shows the effect on execution time caused by employing every t_{PDT} value. As we can see, the overhead caused is similar to values above the nanosecond range, in which 90 % of inactivity periods fit, as shown in Figure 1d. Because that is also the t_w for Fast Wake, we find packet coalescence on output buffers on their way to their destinations, compensating for the overhead. This is why we do not see a steep increase in execution time when very restrictive t_{PDT} values are employed.

Another hint of packet coalescence occurring when using Fast Wake can be seen in Figure 16b. We can see that the latency increase is minimal compared to Deep Sleep.

The benefit of using Deep Sleep instead of Fast Wake is the tradeoff of energy savings for performance. As we can see in Figure 16c, using Deep Sleep leads to more energy savings. The increase in energy saving as the t_{PDT} increases is indicative that the potential for energy saving is hindered by the high number of transitions that occur. This also explains why using a t_{PDT} of 1 second reverts this trend, because then it is unused ports with active PDT timers that prevent energy saving.

4.4.2. Results using PerfBound and PerfBoundCorrect

As we can see in Figure 17a, the results show the same tendencies as with the previous applications. However, this time we manage not only the same reduction in execution time overhead, but we also get that overhead to be below the performance degradation threshold using PerfBoundCorrect.

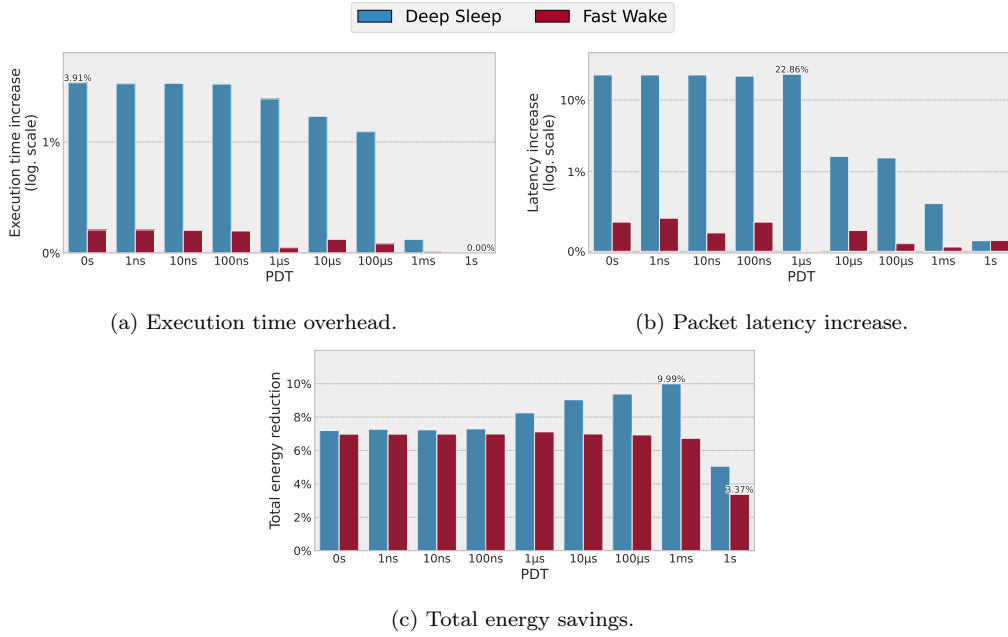


Figure 16: Impact of different t_{PDT} values for ALEXNET.

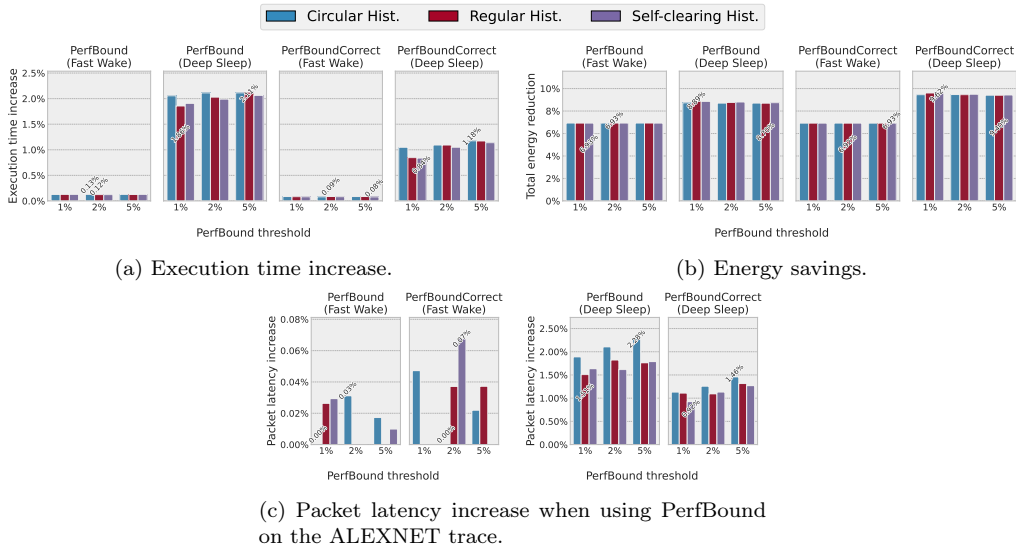


Figure 17: Impact of PerfBound and PerfBoundCorrect on the ALEXNET trace.

Regarding energy savings, we can see that PerfBoundCorrect provides the

same power savings as PerfBound with Fast Wake and a slight improvement using Deep Sleep.

For packet latency, the results are shown in different figures for Fast Wake and Deep Sleep due to the difference in the obtained results. We can see in Figure 17c that even if latency values are worse for PerfBoundCorrect than for PerfBound, the increase is still negligible when the packet latency is within the microsecond scale. Using Deep Sleep, even if the increase is small, we still manage to improve upon PerfBound in all cases.

5. Outcomes and future work

In this work, we have provided a detailed examination of the implications of power in interconnection networks. First, we explored the simplest technique by using fixed t_{PDT} values, which gave us an upper bound for degradation. Later on, we have discussed more sophisticated approaches and solutions that have been proposed, focusing on HPC environments. After careful examination of our own implementation of the PerfBound technique and the results we gathered, we have found several key aspects that could be improved. As we have mentioned in earlier sections, the results are significant compared to the original PerfBound technique, and proves that giving more breathing room it can actually be beneficial to energy efficiency. Furthermore, we also show that other ostensibly trivial aspects like histogram management can have an impact on the energy saved, which was not examined in the original work.

Our observations and experiments have led us to devise a solution to mitigate the implications of using prediction for inactivity periods. Particularly, addressing avoidable prediction misses has proven useful to both performance and energy saving. Indeed, our proposal consistently outperforms PerfBound in terms of performance, while incurring minimal power overhead—or in some cases, even achieving greater energy savings.

Specifically, we have significantly reduced the overhead in terms of execution time and packet latency on the selected applications with minimal sacrifices on energy saving. In the case of the LAMMPS application, we even managed to turn an increment in energy consumption into a reduction.

In our humble opinion, our solution is subject to improvements and several new questions arise. For example, whether providing our dynamic t_{PDT} value calculation with some recency bias would improve the performance on very repetitive patterns.

Acknowledgements. This work has been supported by the Junta de Comunidades de Castilla-La Mancha under projects SBPLY/21/180225/000103, TED2021-130233B-C31 and SBPLY/21/180501/000248, and by the Spanish Ministry of Science and Innovation (MCIN) / Agencia Estatal de Investigación (AEI) under project PID2021-123627OB-C52, co-financed by the European Regional Development Fund (FEDER). We also acknowledge support from the PERTE-Chip grants (UCLM Chair, TSI-069100-2023-0014) from the Spanish Ministry of Digital Transformation and Public Service.

References

- [1] Dennis Abts, Mike Marty, Philip Wells, Peter Klausler, and Hong Liu. Energy Proportional Datacenter Networks. In *Proceedings of the International Symposium on Computer Architecture*, pages 338–347, 2010.
- [2] Francisco J. Andújar, Juan A. Villar, Jose L. Sánchez, Francisco J. Alfaro, and Jesús Escudero-Sahuquillo. VEF Traces: A Framework for Modelling MPI Traffic in Interconnection Network Simulators. In *The 1st IEEE International Workshop on High-Performance Interconnection Networks in the Exascale and Big-Data Era*, pages 841–848, Chicago, IL, USA, Sep 2015.
- [3] Francisco J. Andújar, Juan A. Villar, Jose L. Sánchez, Francisco J. Alfaro, and Jesús Escudero-Sahuquillo. An open-source family of tools to reproduce MPI-based workloads in interconnection network simulators. *Journal of Supercomputing*, 72(12):4601–4628, 2016.
- [4] Francisco J. Andújar, Salvador Coll, Marina Alonso, Juan-Miguel Martínez, Pedro López, José L. Sánchez, and Francisco J. Alfaro. Energy efficient hpc network topologies with on/off links. *Future Generation Computer Systems*, 139:126–138, 2023.
- [5] Francisco J. Andújar, Miguel Sánchez de la Rosa, Jesús Escudero-Sahuquillo, and José L. Sánchez. Extending the VEF traces framework to model data center network workloads. *J. Supercomput.*, 79(1):814–831, 2023.
- [6] Atos. High performance interconnect for extreme HPC workloads. Last accessed: 2022-10-05.

- [7] Hugh Barrass. Options for EEE in 100G IEEE 802.3bj (Draft), September 2012.
- [8] Mark S. Birrittella, Mark Debbage, Ram Huggahalli, James Kunz, Tom Lovett, Todd Rimmer, Keith D. Underwood, and Robert C. Zak. Intel® omni-path architecture: Enabling scalable, high performance fabrics. In *2015 IEEE 23rd Annual Symposium on High-Performance Interconnects*, pages 1–9, 2015.
- [9] Emeric Brun, Stéphane Chauveau, and Fausto Malvagi. Patmos: A prototype monte carlo transport code to test high performance architectures. In *2017 - International Conference on Mathematics and Computational Methods Applied to Nuclear Science and Engineering*, 2017.
- [10] Chelsio Communications. RDMA – iWARP.
- [11] Ken Christensen, Pedro Reviriego, Bruce Nordman, Michael Bennett, Mehrgan Mostowfi, and Juan Antonio Maestro. IEEE 802.3az: The road to energy efficient Ethernet. *Communications Magazine, IEEE*, 48:50 – 56, December 2010.
- [12] Saïd Derradji, Thibaut Palfer-Sollier, Jean-Pierre Panziera, Axel Poudes, and François Wellenreiter Atos. The bxi interconnect architecture. In *Proceedings of the 2015 IEEE 23rd Annual Symposium on High-Performance Interconnects, HOTI '15*, page 18–25, USA, 2015. IEEE Computer Society.
- [13] Branimir Dickov, Miquel Pericàs, Paul Carpenter, Nacho Navarro, and Eduard Ayguade. Software-Managed Power Reduction in Infiniband Links. In *Proceedings of the International Conference on Parallel Processing*, volume 2014, September 2014.
- [14] María Engracia Gómez et al. RED-SEA project: Towards a new-generation european interconnect. *Microprocess. Microsystems*, 110:105102, 2024.
- [15] Eviden SAS. BullSequana eXascale Interconnect V3: Intelligent Network Management Accelerates GPU Performance in AI-HPC. Technical report, Eviden, November 2024.

- [16] Mario Flajslik, Eric Borch, and Mike A. Parker. Megafly: A Topology for Exascale Systems. In Rio Yokota, Michèle Weiland, David Keyes, and Carsten Trinitis, editors, *High Performance Computing*, pages 289–310, Cham, 2018. Springer International Publishing.
- [17] Chamara Gunaratne, Ken Christensen, Bruce Nordman, and Stephen Suen. Reducing the Energy Consumption of Ethernet with Adaptive Link Rate (ALR). *Computers, IEEE Transactions on*, 57:448–461, May 2008.
- [18] Robert Hays. Active/idle toggling with low-power idle. http://www.ieee802.org/3/az/public/jan08/hays_01_0108.pdf, January 2008. Presented at IEEE 802.3az Task Force Meeting, January 2008.
- [19] Jaeha Kim and Mark A. Horowitz. Adaptive supply serial links with sub-1-V operation and per-pin clock recovery. *IEEE Journal of Solid-State Circuits*, 37(11):1403–1413, 2002.
- [20] Jongryoul Kim, William Dally, Brian Towles, and Amit Gupta. Microarchitecture of a High-Radix Router. In *ACM SIGARCH Computer Architecture News*, volume 33, pages 420–431, July 2005.
- [21] Alex Krizhevsky, Ilya Sutskever, and Geoffrey E. Hinton. Imagenet classification with deep convolutional neural networks. *Commun. ACM*, 60(6):84–90, May 2017.
- [22] Michael Langguth, Ankit Patnala, Sebastian Lehner, Markus Dabernig, Konrad Mayer, Irene Schicker, GeoSphere Austria, and Paula Harder. A benchmark dataset for meteorological downscaling. In *International Conference on Learning Representations*, number FZJ-2024-07378. Jülich Supercomputing Center, 2024.
- [23] Md Nahid Newaz, Md Atiqul Mollah, Peyman Faizian, and Zhou Tong. Improving adaptive routing performance on large scale megafly topology. In *2021 IEEE/ACM 21st International Symposium on Cluster, Cloud and Internet Computing (CCGrid)*, pages 406–416, 2021.
- [24] NVIDIA Corporation. RoCE vs. iWARP Competitive Analysis (Whitepaper), February 2017.

- [25] Pedro Reviriego, José Alberto Hernandez, David Larrabeiti, and Juan Antonio Maestro. Performance evaluation of energy efficient ethernet. *IEEE Communications Letters*, 13(9):697–699, 2009.
- [26] Efraim Rotem, Alon Naveh, Avinash Ananthakrishnan, Eliezer Weissmann, and Doron Rajwan. Power-Management Architecture of the Intel Microarchitecture Code-Named Sandy Bridge. *IEEE Micro*, 32(2):20–27, 2012.
- [27] Karthikeyan Saravanan, Paul Carpenter, and Alex Ramirez. Power/performance evaluation of energy efficient Ethernet (EEE) for High Performance Computing. In *ISPASS 2013 - IEEE International Symposium on Performance Analysis of Systems and Software*, pages 205–214, April 2013.
- [28] Karthikeyan P. Saravanan and Paul M. Carpenter. Perfbound: Conserving energy with bounded overheads in on/off-based hpc interconnects. *IEEE Transactions on Computers*, 67(7):960–974, 2018.
- [29] Alexander Sergeev and Mike Del Balso. Horovod: fast and easy distributed deep learning in TensorFlow. *CoRR*, abs/1802.05799, 2018.
- [30] Li Shang, Li-Shiuan Peh, and N.K. Jha. Dynamic voltage scaling with links for power optimization of interconnection networks. In *The Ninth International Symposium on High-Performance Computer Architecture, 2003. HPCA-9 2003. Proceedings.*, pages 91–102, 2003.
- [31] Alexander Shpiner, Zachy Haramaty, Saar Eliad, Vladimir Zdornov, Barak Gafni, and Eitan Zahavi. Dragonfly+: Low cost topology for scaling datacenters. In *2017 IEEE 3rd International Workshop on High-Performance Interconnection Networks in the Exascale and Big-Data Era (HiPINEB)*, pages 1–8, 2017.
- [32] Physical Layer Specifications. *IEEE Draft P802. 3az™/D2.*, 2009.
- [33] Estela Suarez, Norbert Eicker, and Thomas Lippert. *Modular Supercomputing Architecture: from Idea to Production; 3rd*, volume 3, pages 223–251. CRC Press, FL, USA, 2019.
- [34] Top500.org. Green500 list.

- [35] Top500.org. Top500 list. Last accessed: 2025-06-17.
- [36] Juan Antonio Villar, German Maglione Mathey, Jesús Escudero-Sahuquillo, Pedro Javier García, Francisco J. Alfaro, José Luis Sánchez García, and Francisco J. Quiles. Topgen: A library to provide simulation tools with the modeling of interconnection network topologies. In *2018 International Conference on High Performance Computing & Simulation, HPCS 2018, Orleans, France, July 16-20, 2018*, pages 452–459. IEEE, 2018.
- [37] Pedro Yébenes, Jesus Escudero-Sahuquillo, Pedro J. García, Francisco-J. Alfaro-Cortés, and Francisco J. Quiles. Providing differentiated services, congestion management, and deadlock freedom in dragonfly networks with adaptive routing. *Concurrency and Computation: Practice and Experience*, 29(13):e4066, 2017.
- [38] Eitan Zahavi. Fat-trees routing and node ordering providing contention free traffic for MPI global collectives. *Journal of Parallel and Distributed Computing*, 72, 05 2011.
- [39] Yibo Zhu, Haggai Eran, Daniel Firestone, Chuanxiong Guo, Marina Lipshteyn, Yehonatan Liron, Jitendra Padhye, Shachar Raindel, Mohammad Haj Yahia, and Ming Zhang. Congestion control for large-scale RDMA deployments. In *Proceedings of the 2015 ACM Conference on Special Interest Group on Data Communication*, page 523–536, 2015.